CONTRACT NO. 952249

ACTION OF LITHIUM IN RADIATION-HARDENED SILICON SOLAR CELLS

FIRST QUARTERLY REPORT

Prepared for

JET PROPULSION LABORATORY
CALIFORNIA INSTITUTE OF TECHNOLOGY
PASADENA, CALIF.

BY

G.J. BRUCKER, T.J. FAITH, AND A.G. HOLMES-SIEDLE

RCA Astro Electronics
Princeton, New Jersey

AED R-3363

ISSUED: AUGUST 15, 1968

CONTRACT NO. 952249

ACTION OF LITHIUM IN RADIATION-HARDENED SILICON SOLAR CELLS

FIRST QUARTERLY REPORT

Prepared for

Jet Propulsion Laboratory
California Institute of Technology
Pasadena, Calif.

By

G.J. Brucker, T.J. Faith, and A.G. Holmes-Siedle

RCA Astro Electronics
Princeton, New Jersey

This work was performed for the Jet Propulsion Laboratory, California Institute of Technology, as sponsored by the National Aeronautics and Space Administration under Contract NAS7-100.

AED R-3363

Issued: August 15, 1968

NOTICE

This report contains information prepared by the Astro-Electronics Division of RCA under JPL subcontract. Its content is not necessarily endorsed by the Jet Propulsion Laboratory, California Institute of Technology, or the National Aeronautics and Space Administration.

PREFACE

This is the First Quarterly Report on a program to study the "Action of Lithium in Radiation-Hardened Silicon Solar Cells." This report was prepared under Contract No. 952249 for Jet Propulsion Laboratories, Pasadena, California by the Astro-Electronics Division of RCA, Princeton, New Jersey. The period of performance covered by this report is from April 23 to July 15, 1968.

ABSTRACT

This is the First Quarterly Report on a program to study and analyze the action of lithium in producing a recovery of radiation damage in silicon solar cells. This program has technical continuity with the work performed for NASA on Contract No. NAS5-10239. The eventual goal of this effort is to understand the recovery mechanism so that realistic predictions of solar-cell performance can be developed and optimum designs of lithium cells for space use can be specified.

The test vehicles being used for this work are (1) small-area solar-cell model devices, (2) a group of solar-cells supplied by NASA on the above contract, (3) high-performance solar cells supplied by JPL and (4) silicon bars, usually in the "Hall-bar" configuration. The source of particle irradiation being used is a 1-MeV electron beam produced by the RCA Laboratories Van de Graaff generator.

Technical progress during this reporting period includes stability data which are now available for some cells for periods ranging to approximately two years. The post-irradiation data, obtained after fluences of 10^{14}, 10^{15}, and 10^{16} e/cm^2, indicates that post-recovery redegradation is most severe after 10^{14} e/cm^2. After 10^{15} and 10^{16} e/cm^2, recovery is less complete but redegradation less severe. Over an 18-month period, redegradation phenomena in lithium-containing solar cells can vary from insignificant in magnitude to very serious. A definite superiority of Float-Zone-refined silicon over Lopex silicon is seen; the few samples tested indicate that Quartz-Crucible silicon, while producing a much slower recovery than the other two, shows minimal redegradation over 18 months. High lithium concentrations are definitely to be avoided.

It is not yet clear how the diffusion constant of lithium measured near the junction is related to that deduced for the whole ($\sim$ 200-micrometer) collection region of the cell. It appears that lattice damage is present in the junction depletion region even before irradiation and that this can be useful in stabilizing lithium in the cell.

Hall and resistivity measurements indicate that carrier-removal rates at low temperatures are lower in lithium-doped silicon than in phosphorus-doped silicon, which also contains oxygen. This may mean that the affinity of vacancies for lithium is less than that for phosphorus, a fact which is in agreement with earlier experiments. The interaction of lithium with vacancies has definitely been observed in recent work and the data will be of great use in improving and detailing the current models for damage to solar-cell performance at any temperature.

TABLE OF CONTENTS

TABLE OF CONTENTS (Continued)

LIST OF ILLUSTRATIONS

LIST OF TABLES

SECTION I

INTRODUCTION

A. GENERAL

It has been shown that electron, proton, and neutron-irradiated silicon solar cells spontaneously recover at room temperature their electrical outputs following irradiation (Reference 1). Initially, the loss of electrical output is due to degradation of minority-carrier lifetime. The mobile lithium ion moves to and combines with a defect-impurity complex, thereby changing its electrical properties. In solar cells, the interaction of lithium with radiation-induced defects produces a defect complex which appears to have little or no effect on the minority-carrier lifetime.

This contract effort represents an experimental investigation of the physical properties of lithium-containing p-on-n silicon solar-cells and of the processes which occur in these devices before and after irradiation. Its objectives are to identify the parameters which affect cell radiation recovery and long-term stability characteristics and to generate information which will lead to the optimization of these parameters. The eventual goal is to exploit this phenomenon for adaptation to the production of solar cells for the space environment. In this direction, it is anticipated that (1) realistic predictions of lithium cell performance can ultimately be developed, and (2) optimum designs of lithium cells for space use can then be specified.

B. TECHNICAL APPROACH

Stated briefly, the approach to the objectives involves the testing of bulk samples as well as government furnished (GFE)[1] solar-cells and in-house fabricated test-diodes[2]. Experiments on bulk samples include Hall and resistivity measurements taken as functions of (1) 1-MeV electron fluence (2) sample temperatures during irradiation, and (3) isochronal anneals. Correlations of these tests will be made wherever possible with measurements on solar-cells and test-diodes. These measurements will include minority-carrier diffusion length versus (1) fluence, (2) temperature, and (3) annealing schedule; photovoltaic I-V characteristics; and reverse-bias capacitance measurements. In addition, stability tests are being continued on test-diodes and solar-cells with post-irradiation histories dating back as far as December 1966.

---

[1] *Government Furnished Equipment (by NASA under Contract No. NAS5-10239 and JPL under this contract).*

[2] *Test vehicles, similar to solar cells in all but photovoltaic response, fabricated to be compatible with experiments which appear particularly promising in terms of information yield as well as the experiments which are regularly performed in the course of the work.*

C. SUMMARY OF RECENT PREDECESSOR WORK (Late 1967 to Mid 1968)

A brief history is given here of the recent work performed on a predecessor contract[3] for purposes of continuity, and to provide the reader with a better understanding of the current technical approach, its problems and its objectives.

In the work of the past year, in addition to continuing and extending a series of long-term stability tests on GFE[1] cells to in-house fabricated test-diodes[2] and to a new group of GFE[1] cells, extensive measurements of cell capacitance were made over a wide range of reverse biases. These measurements, which yield donor-density vs. distance from the junction, uncovered large lithium density gradients ($\sim 10^{19}$ cm^{-4}) near the junction and extending (≥ 10 μm) from the junction. This gradient sets up a large internal electric field (> 100 V/cm near the junction edge) thereby creating a field-aided diffusion situation for minority-carriers. This effect invalidates the concept of diffusion length for small lifetimes, i.e., where the electric field effect is significant over a large fraction of the current-collection volume. This is the case after irradiation to fluences of the order 10^{15} to 10^{16} MeV/cm^2, making application of Waite's theory (Reference 2) very difficult. Accordingly, in the past year, some kinetic studies of damage recovery were made at lower fluences, in the range 10^{13} to 10^{14} e/cm^2. Waite's theory, which reduces to a first-order kinetic equation at these fluences, was shown to describe the experimental recovery curves adequately for a large number of cells. These cells and cells irradiated to $\sim 10^{15}$ e/cm^2, as well as unirradiated cells, have since been undergoing long-term monitoring of their characteristics for (1) stability, (2) minority-carrier diffusion length, and (3) photovoltaic I-V characteristics. These stability tests have continued into the present contract and it is planned that they will continue throughout the duration of this effort. The cumulative results are presented and discussed in Section III of this Report.

In the past year, the first known use was made of capacitance techniques for direct measurement of the lithium diffusion constant in a solar cell (Reference 3). Results obtained by using this technique have indicated the possibility that the lithium diffusion constant at the edge of the junction, where the measurements are made, is often lower than that in the bulk of the current-collection volume. To clarify this question, which will have significant consequences in the understanding of cell stability, an attempt is being made to probe further into the base region of the cell by use of the capacitance method. The theoretical basis for the extension of such measurements is outlined in Section IV of this report.

In addition to the fabrication of many test diodes, the effort in the past year was directed toward modifying an existing apparatus for Hall measurements at liquid nitrogen temperature and to the fabrication, lithium diffusion, and contacting of appropriate Hall samples. The purpose of these measurements is to obtain information on the

---

[3] *"Radiation Damage in Lithium-Containing Solar Cells," Contract No. NAS5-10239, Performed for the National Aeronautics and Space Administration, Goddard Space Flight Center, Greenbelt, Md. Final Rept. Issued July 1968.*

defect formation and annealing processes occurring in the lithium cell and the band-gap energy levels occurring in these processes. Actual Hall measurements were started toward the end of Contract NAS5-10239[3]. These measurements are presently being pursued, and some preliminary results are given and discussed in Section V. This work was planned to be closely coordinated with the studies of annealing of minority-carrier damage in cells made from exactly similar material. Correlations will then be sought throughout these sets of measurements. As a part of this effort, a cold-finger apparatus has been constructed to enable cell (and test-diode) measurements to be made at temperatures as low as liquid-nitrogen. Measurements of diffusion length, cell capacitance, and, if possible, pulsed minority-carrier lifetime will be made and related to the bulk sample measurements of photoconductive decay. The design of this apparatus is described in Section V.

SECTION II

TEST VEHICLE FABRICATION

A. DIODES

In 1966-68, under Contract NAS5-10239, several dozen test diodes, both lithium-containing and non-lithium-containing "control" devices were fabricated and subjected to irradiation and electrical measurements (Reference 4). In addition to continuing experiments on these diodes, a new set of test-diodes is presently being fabricated. The new group of devices will, as before, provide a close model of the junction structure used in solar cells but, as a new feature, will be well-adapted for diffusion-length measurements at the temperature of liquid-nitrogen as at room temperature. The diodes, as shown in Figure 1, are being made from high-resistivity (nominal 1900 Ω-cm) n-type Float-Zone Silicon. The use of this material assures that the principle electrically active impurity in the base region is lithium. A p-n junction is made by diffusion of boron from a deposited 3000Å layer of 10-percent borosilicate glass at 1150°C for 15 minutes.

Two different lithium-diffusion schedules have been used on different wafers. In each case, a wafer is immersed in a 1-percent lithium-tin bath. These are, (a) an $\sim$ 70-hour diffusion at 325°C and (b) a 2-hour diffusion at 375°C. Four-point probe measurements (Reference 5) on the back surfaces of each wafer indicated a resistivity of $\approx 1.5\ \Omega$-cm, which is equivalent to a bulk lithium density of $\approx 4 \times 10^{15}$ cm^{-3}. The ≈ 0.025-inch thick wafers were cut into four 0.25 x 0.40-inch cells and at the close of this reporting period solderable contacts were being applied. The base contact will be an alloyed Au-Sb contact; the contact to the p-skin will be a $\sim$3000A chrome-gold evaporated layer. The cells will be soldered onto a 0.020-inch thick metallized boron-nitride wafer. The boron-nitride wafer will be soldered onto a cold finger which has been designed to fit onto the beam exit of the Van de Graaff generator. This apparatus will permit capacitance, diffusion-length, and possibly pulsed-lifetime measurements on test-diodes and solar-cells as a function of electron fluence and temperature. The cold finger is described in Section V.

B. HALL BARS

The Hall bars were diffused with lithium under approximately the same conditions as were employed for the test diodes, the times being adjusted to give the desired lithium concentrations. As of the end of this reporting period, several Hall bar

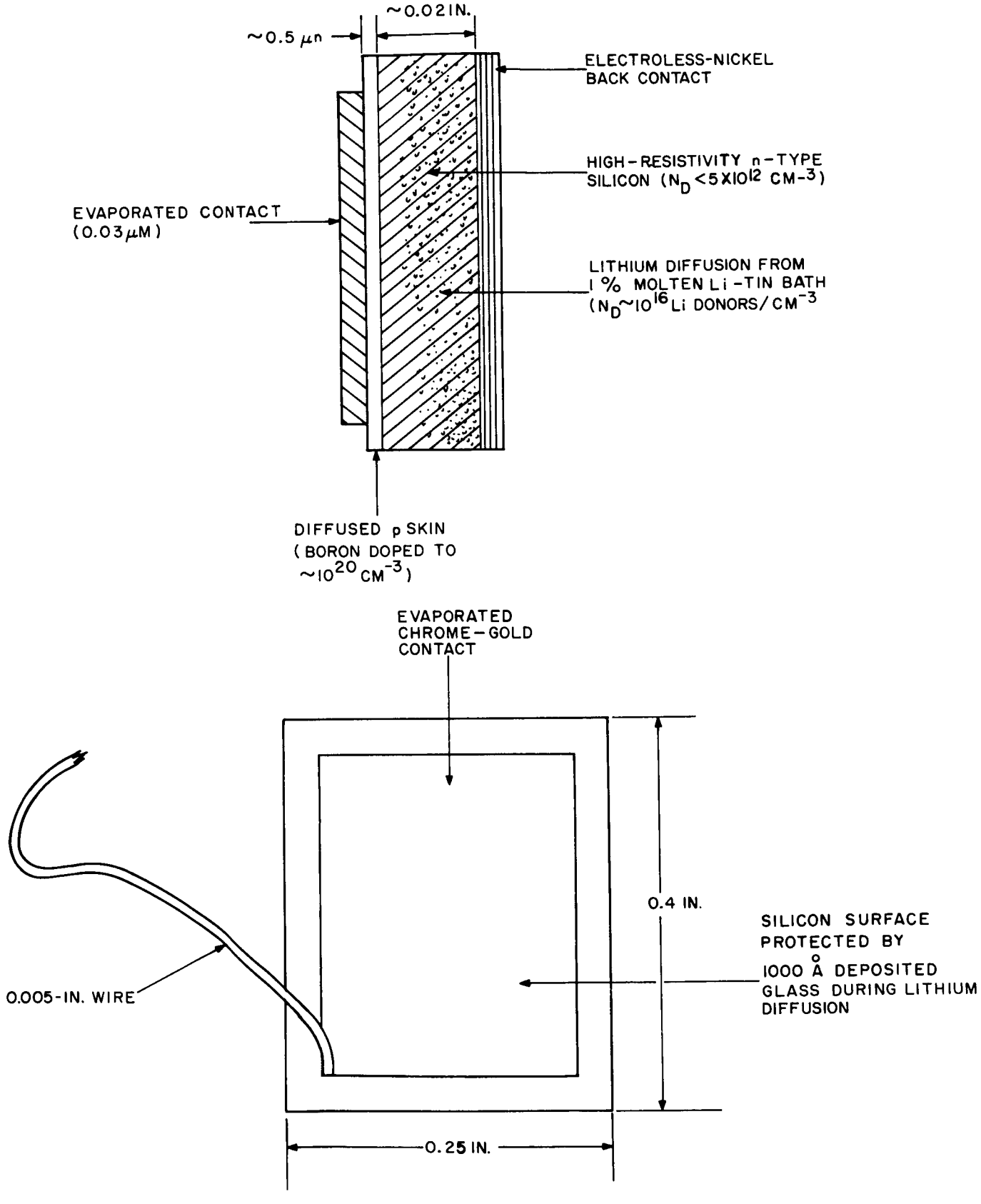

Figure 1. Construction of Test Diode

samples were constructed. Sample No. 1 was doped with a lithium concentration of $\approx 2 \times 10^{15}$ Li atoms/cm^3 ($\rho = 2.5\Omega$-cm) and Sample No. 2 with a concentration of $\approx 1.8 \times 10^{16}$ Li atoms/cm^3 ($\rho = 0.3\Omega$-cm). The geometry and dimensions of the silicon Hall bars are shown in View A of Figure 2. A magnetic field strength of 1600 gauss and currents ranging from 1 to 3 milliamperes were used to make the measurements. The starting material for both samples before diffusion with lithium was 30 Ω-cm phosphorus-doped silicon. Lithium diffusion was accomplished by heating the starting material in a 1-percent lithium-tin bath at 400°C for several days. After suitable cleaning processes, the silicon wafers were cut ultrasonically into the shape shown in View A. Ohmic contacts were made on the bars by alloying the silicon with 1-percent arsenic-tin or 1-percent antimony-gold alloy. Final connection to the alloy dot was made by soldering one end of a fine gold wire to the dot with indium solder and the other end to the indium-tinned gold pattern on the ceramic substrate which provided an insulated base for mounting the samples. The gold pattern was fixed to the ceramic substrate by the standard molybdenum silk-screen process. A thermally conductive epoxy was used to attach the Hall bar to the ceramic substrate and the ceramic substrate to a copper plate. Six leads of 0.005-inch-diameter formvar wire were soldered to the six contacts on the ceramic substrate and a copper-constantan thermocouple was cemented to one of the arms of the bar, as shown in View B of Figure 2.

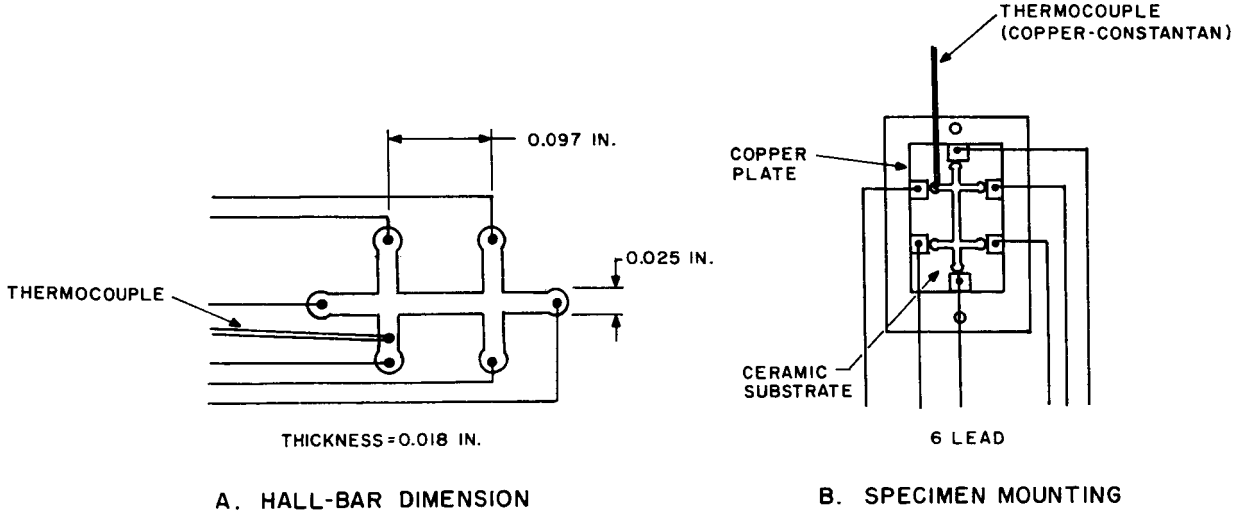

Figure 2. Hall Bar Geometry and Specimen Mounting

SECTION III

STABILITY OF GFE CELLS

A. GENERAL

A large group of solar cells furnished under Contract No. NAS5-10239[1] and irradiated to various fluences by 1-MeV electrons have been remeasured for photovoltaic I-V characteristics during this reporting period. The cells were illuminated by a filtered tungsten light adjusted to an incident power of 100 mW/cm^2 at the front surface of the cells. These tests represent a continuing accumulation of stability data on cells irradiated in the time period between December 1966 and March 1968. In addition, a group of unirradiated cells have been tested for shelf-life stability since November 1967. In a large percentage of these tests the minority-carrier diffusion length (Reference 6) was also measured. However, due to the large volume of data acquired, only the most important cell performance parameters, namely maximum power and short circuit current, will be reported here. In each of the tables to appear below, a running account is given from the initial (pre-irradiation) set of measurements to those taken during the present reporting period. The results on the unirradiated cells will be presented first, followed by those on the irradiated cells, which will be presented in chronological order as to the date of irradiation. This Section will be concluded by a discussion of the results, including an attempt to relate cell stability to cell physical parameters. The long-term reproducibility of the I-V measurements, as measured on "control" cells has been found to be within ±5 percent, thus the data in the tables of this section exhibit this degree of uncertainty.

B. UNIRRADIATED CELLS

Table I presents a performance history for nineteen Heliotek (He) cells and two Texas Instruments (TI) cells covering eight months and beginning with the first measurement on the cells. These unirradiated cells have been stored in open-circuit condition at room temperature under the illumination of room light (fluorescent) except for short periods (~ minutes) when the cells were biased for capacitance measurements, and during photovoltaic I-V measurements. In addition, a negligibly small electron fluence was applied to each cell during minority-carrier diffusion-length measurements. This fluence is calculated to be less than 10^{10} e/cm^2. All of the solar cells were fabricated from phosphorous-doped n-type silicon ingots with the addition, through diffusion, of the lithium donor. The fabrication details for these cells, as for the other GFE cells discussed in this report, are presented in Heliotek (Reference 7) and Texas Instruments (Reference 8) status reports.

TABLE I. PERFORMANCE HISTORY OF UNIRRADIATED CELLS

Sample No.	ρ_o and Growth Method	November 1967		March 1968		July 1968	
		J_{sc} (mA/cm^2)	P_{max} (mW/cm^2)	J_{sc} (mA/cm^2)	P_{max} (mW/cm^2)	J_{sc} mA/cm^2)	P_{max} (mW/cm^2)
He 673	20 L	24.3	8.8	25.0	9.4	23.1	8.5
676	20 L	25.9	9.1	26.6	9.7	24.7	8.0
694	20 L	25.8	9.4	26.8	9.7	24.9	8.5
796	20 FZ	26.0	9.5	26.9	10.3	25.2	9.4
808	20 FZ	26.4	9.6	27.2	10.0	25.8	9.5
815	20 FZ	28.3	11.0	29.1	8.5	27.7	11.0
866	20 FZ	29.0	10.8	30.2	11.5	29.0	11.0
867	20 FZ	28.6	10.7	29.9	11.8	28.5	10.8
868	20 FZ	26.5	9.9	28.0	10.7	26.6	10.0
870	20 FZ	28.0	10.5	29.6	11.2	28.5	10.8
871	20 FZ	29.6	11.2	31.6	12.4	30.5	12.0
872	20 FZ	-	-	28.0	10.6	27.1	10.2
873	20 FZ	29.0	11.6	30.0	11.4	29.0	11.1
875	20 FZ	28.1	10.7	29.1	10.9	27.8	10.3
876	20 FZ	27.6	9.6	28.6	11.0	27.5	10.5
878	20 FZ	28.3	11.1	26.1	11.2	28.2	10.8
886	20 FZ	29.1	10.7	30.4	11.5	29.5	11.2
887	20 FZ	30.6	10.8	31.8	11.4	30.7	10.9
892	20 FZ	28.9	11.0	29.8	11.4	29.0	11.6
TI 976	200 L	32.0	12.1	33.8	12.9	32.5	11.8
979	200 L	32.4	11.8	34.3	11.0	33.2	8.4

NOTES: 1. L is Lopex
2. FZ is Float Zone

All of the Heliotek cells shown in Table I were fabricated from 20 ohm-cm starting material. The two TI cells were fabricated from 200 ohm-cm Lopex[4] silicon. Three of the Heliotek cells were fabricated from Lopex silicon, the remaining sixteen were from Float-Zone silicon.

Comparison of the initial power measurements, taken in November, 1967, with those taken four months later in March 1968, indicates that for 20 cells (no measurement was taken in November on He 872; the March power measurement on He 815 is considered in error, probably due to faulty contacts, and is therefore not accounted for in the average) the calculated average power has increased from 10.5 to 11.0 mW/cm, an increase of less than 5 percent. Thus, for this period, the cells as a group are regarded as having maintained constant power within experimental uncertainty. Only two cells (excluding He 815) showed decreases in power, these being 2 percent for He 873 and 8 percent for TI 979, both being within the ±5 percent uncertainty. All of the other cells showed slight increases, in power; some appearing real; only in one case was this increase greater than 10 percent, i.e., He 876 was 14 percent.

[4] *Texas Instruments Tradename*

The average power value for the 21 cells, determined in July 1968, was 10.3 mW/cm^2, which is well within the ±5 percent uncertainty with respect to the previous readings. However, where the cells are considered individually, two cells: He 676 and TI 979, show greater than 10-percent decreases in power when compared with the initial readings. Furthermore four cells, the two just noted plus He 673 and He 694 show greater than 10-percent decreases between March and July. All of the cells displaying this degradation were fabricated from Lopex silicon. None of the Float-Zone cells have degraded beyond the experimental uncertainty. Thus, as will be discussed later, some real changes appear to have taken place.

C. IRRADIATED CELLS

1. Cells Irradiated to 10^{14} e/cm^2 in December 1966

Four Float-Zone cells of various starting resistivities have been under investigation since December 1966. These are represented in Table II, where pre-irradiation or initial values are listed, followed by a running account of measurements to date. The cells prefixed with "HO" were manufactured by Hoffman Electronics Corporation (Reference 9). It may be seen that Sample No. He 55-1 had significantly higher initial values than the other cells and that all cells showed practically complete recovery in photo-response. The photo-response parameters after recovery remained constant within 10 percent from December 1966 through June 1967. Severe post-recovery re-degradation in power (approximately 50 percent) in cell 55-1, which was observed in the November 1967 reading occurred between 6 and 11 months after recovery, and was accompanied by only slight decreases in short-circuit current and open-circuit voltage, and no decrease in diffusion length. A decrease in filling factor, $P_{max}/J_{sc}V_{oc}$, was responsible for the power drop, indicating that a contact problem was responsible. The Hoffman cells have remained stable at the post-recovery values for over 18 months, with a slight upward trend evident in Samples No. HO 5-1 and HO 6-1. It is noted that reverse-bias capacitance measurements (Reference 10) made before irradiation indicated that the lithium density, N_{LD} at a distance of approximately 1 micrometer from the junction was

He 55-1	1.7×10^{15} cm^{-3}
HO 33-2	1.5×10^{14} cm^{-3}
HO 5-1	2.4×10^{14} cm^{-3}
HO 6-1	4.3×10^{14} cm^{-3}

Thus, the cells with good long-term stability after a fluence of 10^{14} e/cm^2 were very lightly doped with lithium.

TABLE II. POST-IRRADIATION STABILITY OF PERFORMANCE PARAMETERS FOR GFE CELLS IRRADIATED IN DECEMBER 1966

Sample No.	ρ_o and Growth Method	Initial Performance 12/66		Fluence 12/16/66 ø	After Recovery			
					December 1966		January-February 1968	
		J_{sc} (mA/cm^2)	P_{max} (mW/cm^2)		J_{sc}	P_{max}	J_{sc}	P_{max}
HE55-1	20 FZ	29.2	9.2	10^{14}	26.4	9.0	26.5	8.3
HO33-2	10 FZ	24.4	6.6	10^{14}	23.1	6.2	24.6	6.3
HO5-1	100 FZ	24.7	7.7	10^{14}	25.0	8.0	24.7	7.6
HO6-1	1000 FZ	23.3	6.4	10^{14}	23.3	8.0	23.1	7.5

Sample No.	After Recovery (Cont'd)							
	June 1967		November 1967		March 1968		July 1968	
	J_{sc}	P_{max}	J_{sc}	P_{max}	J_{sc}	P_{max}	J_{sc}	P_{max}
HE55-1	25.0	8.3	24.9	4.4	26.2	4.9	26.0	4.4
HO33-2	22.8	6.6	23.4	6.2	25.0	6.9	25.0	6.7
HO5-1	25.0	7.7	24.0	8.0	26.6	8.5	26.8	8.5
HO6-1	24.5	8.4	24.9	8.6	26.2	9.1	26.0	8.8

Note: FZ is Float Zone

2. Cells Irradiated to 10^{16} e/cm^2 in February-March 1967

During February and March, 1967, a large number of government-furnished cells were irradiated to 10^{16} e/cm^2 at a flux rate of approximately 3 x 10^{15} e/cm^2/hr. Periodic measurements of diffusion lengths and photo-response characteristics were made. Table III lists values of J_{sc} and P_{max} obtained from these measurements. Readings made before bombardment and approximately one hour, four days, three months, eight months, one year, and 16 months after bombardment are included. Pre-irradiation values of lithium concentration (lithium ions/cm^3) near the junction ($\sim 1\,\mu$m), taken from reverse-bias capacitance measurements (Reference 10) were found in early work under contract NAS 5-10239 (Reference 11) and the cells were listed in order of increasing lithium concentration. In more recent work under NAS 5-10239 (Reference 4) the cells were placed in three categories as to lithium concentration. Table III lists the cell performance histories according to this categorization which is as follows: The first group of five cells had initial lithium concentrations less than 2 x 10^{15} cm^{-3}; the second group of six cells had concentrations between 2 and 5 x 10^{15} cm^{-3}; the third group of four cells had concentrations between 7 and 10 x 10^{15} cm^{-3}. A fourth group of two cells, He 248P and He 249P, represent a special group of cells with a diffused heavily doped phosphorous region near the junction.

Two of the cells belonging to Group 1 (TI 63 and TI 171) have recovered in J_{sc} and P_{max}, slowly, but steadily since bombardment. The low lithium density is probably responsible for the slow recovery. At the end of the reporting period, these two cells had values of $P_{max} \sim 4.5$ mW/cm^2 and presumably will continue to increase towards the ~ 5.2

TABLE III. CELLS IRRADIATED TO 10^{16} e/cm^2 IN FEBRUARY-MARCH 1967

Sample No.	ρ_o and Growth Method	Initial Measurement (December 1966)		Post-Irradiation Measurements											
				1 Hour		4 Days		June 1967		November 1967		February 1968		July 1968	
		J_{sc}	P_{max}	J_{sc}	P_{max}	J_{sc}	P_{max}	J_{sc}	P_{max}	J_{sc}	P_{max}	J_{sc}	P_{max}	J_{sc}	P_{max}
TI 167	20 FZ	30.8	10.8	10.8	2.3	10.9	2.2	12.9	3.0	14.5	2.9	15.4	3.2	15.1	3.2
He 342	100 FZ	29.6	-	-	-	-	-	18.3	-	19.6	3.3	21.5	4.1	21.0	3.5
TI 63	20 FZ	29.6	10.4	9.5	2.0	11.2	2.1	15.7	3.4	17.6	3.9	19.3	4.5	19.3	4.6
TI 171	20 FZ	28.5	6.3	9.4	1.6	11.6	1.8	16.2	2.8	18.7	3.7	20.6	4.3	20.6	4.5
He 341	100 FZ	28.5	-	-	-	-	-	21.0	-	20.4	2.6	22.0	3.3	20.0	2.4
TI 112	20 QC	28.0	10.5	9.5	2.5	10.2	2.7	17.4	4.0	19.7	4.9	20.6	5.6	20.7	5.9
TI 113	20 QC	27.5	9.9	9.2	2.5	9.8	2.7	16.8	-	19.0	5.2	20.2	5.8	19.7	5.6
TI 168	20 FZ	28.8	11.1	9.9	2.5	13.5	3.3	16.7	4.0	17.6	4.4	18.6	4.8	18.0	4.6
He 340	100 FZ	28.6	-	-	-	-	-	21.2	-	21.2	2.9	22.9	3.8	21.5	3.0
TI 42	20 FZ	28.6	9.2	8.3	2.0	12.2	3.0	15.1	3.9	16.3	4.2	17.2	4.6	16.2	4.3
TI 161	20 FZ	27.2	10.8	8.9	2.6	17.1	5.1	17.4	5.3	17.4	5.5	18.2	5.8	17.1	5.4
TI 128	20 L	28.5	10.8	9.1	2.5	16.7	5.0	16.0	4.9	15.7	3.4	16.2	3.6	15.4	4.0
TI 127	20 L	30.2	10.2	9.4	2.6	17.8	5.2	16.9	4.9	15.3	3.0	13.8	2.7	14.7	2.9
TI 132	20 L	29.8	-	10.7	1.5	16.2	4.8	15.2	4.1	15.8	4.0	16.2	4.1	15.1	3.7
TI 166	20 FZ	25.2	8.7	9.6	2.5	15.8	4.5	14.8	4.2	15.1	4.1	15.5	4.1	14.9	3.9
He 248P	1000 FZ	24.8	8.4	16.6	3.8	22.3	6.1	22.5	5.0	22.2	6.3	23.5	7.0	23.0	6.7
He 249P	1000 FZ	24.2	8.4	14.2	3.5	20.6	5.7	23.7	6.3	22.2	6.9	22.8	7.4	22.2	7.3

NOTES: 1. J_{sc} *is measured in mA/cm*^{2}
2. P_{max} *is measured in mW/cm*^{2}
3. *FZ is Float Zone*
4. *QC is Quartz-Crucible*
5. *L is Lopex*

mW/cm^2, as reported for a 10 Ω-cm n/p cell (Reference 12) after 10^{16} e/cm^2 bombardment. Cell TI 167, however, has shown no significant recovery since June (~ 3 mW/cm^2), and it must be assumed that this cell, which had the lowest initial lithium concentration of all the cells in this test, has exhausted its free lithium supply near the junction and consequently will recover no further. Cells He 341 and He 342 (and also He 340 of Group 2) display interesting features. These three cells, which were made from high resistivity (100 Ω-cm) starting material showed good recovery of minority-carrier lifetime, as seen from diffusion-length measurements and J_{sc} measurements. In November, He 341 had the highest diffusion length (21 μm) of the cells in Group 1, and cell He 340 the highest in Group 2 (18 μm). From Table III it can be seen that these three cells also have the highest values of J_{sc} relative to the other cells in Groups 1 and 2. In spite of this, they have three of the lowest values of P_{max} of the cells in Groups 1 and 2; the only P_{max} reading below these being that for TI 167, a cell with presumably no free lithium remaining. The reason for this low power is the very low filling factor, $P_{max}/J_{sc}V_{oc} \sim 0.4$, found in the photo-response curves of these cells. This low filling factor is attributed to the high resistivity starting material, which, together with the high bombardment fluence, results in a low post-irradiation-impurity concentration. This could lead to problems either in series resistance at the base contact or in parts of the body of the cell where lithium was heavily depleted. The other cells of Groups 1 and 2 (with 20 Ω-cm starting material) had significantly higher filling factors, suggesting that series resistance problems can be

adequately dealt with by judicious choice of initial silicon resistivity. This observation goes far in answering some objections to the lithium cell (Reference 13).

Group 2 cells with "intermediate" (2 to 5 x 10^{15} cm^{-3}) lithium concentrations near the junction differ from Group 1 cells in their post-irradiation behavior only in degree. They show consistent and continuing recovery just as do Group 1 cells, however, due to the higher lithium density, the recovery has been more rapid and these cells (excepting cell He 340, discussed above) now display values of P_{max} comparable to that obtained for 10 Ω-cm n/p cells (Reference 12) irradiated to 10^{16} e/cm^2. In fact, cell TI 166, of this group with the highest initial lithium concentration (5 x 10^{15} cm^{-3} near the junction) recovered to a power of greater than 5 mW/cm^2 as early as June 1967. This recovery is significant in that the radiation dose of 10^{16} e/cm^2 of 1 MeV electrons is the equivalent of several year's dose in a particularly high-radiation Earth orbit. It is particularly interesting to compare the time behavior of the two quartz-crucible cells (TI 112 and TI 113) of this group with that of the float-zone cells (TI 42, TI 161 and TI 168). This comparison is made in Figure 3, which is a graphic representation of the P_{max} values in Table III. The solid and dotted lines represent the average values for Quartz-Crucible and Float-Zone cells respectively. The slow but steady increase in Quartz-Crucible cell performance stands out in contrast to the rapid initial increase followed by a very slow long-term increase in the performance of Float-Zone cells. As of the last measurements, the quartz-crucible cells are significantly (> 10 percent) ahead of the Float-Zone cells in power output. The contrasting initial behavior has been reported (References 14 and 15) and explained

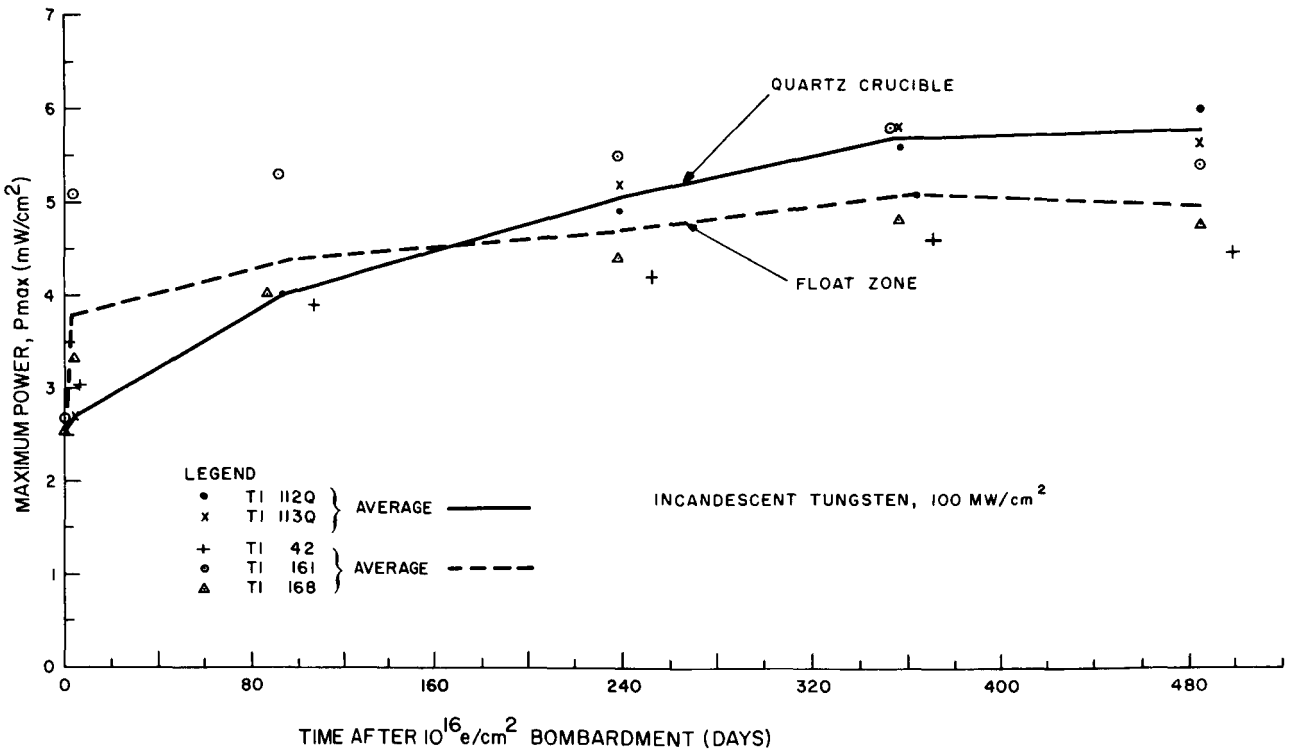

Figure 3. Comparison of the Time Behavior of Two Quartz-Crucible and Three Float-Zone Cells

previously (Reference 14) in terms of formation of LiO^+ complexes which lower the effective lithium diffusion constant in oxygen-rich Quartz-Crucible cells. The observed long-term behavior of the Quartz-Crucible cells also agrees with this observation. The even-slower long-term recovery in Float-Zone cells could be explained in two different ways: first, the rapid initial flow of lithium to defects could cause local depletion of lithium near the junction, leaving some recombination centers after the initial fast recovery unsatisified in their demand for lithium. Lithium would have to diffuse across large distances to satisfy these centers. A second, and more likely, explanation is that over the long-term recovery has to compete with some redegradation mechanism, i.e., recovery and redegradation mechanisms may be occurring simultaneously. Post-recovery redegradation of performance in lithium-doped cells has been observed here (e.g., Group 3 of the cells in Table III) and elsewhere (Reference 15) and its cause, although not well understood, has been suggested to be the precipitation of lithium from the supersaturated solution that exists in the lithium-doped p/n silicon cell. (The solubility of lithium at room temperature in n-type silicon is $\sim 10^{13}$ cm^{-3}.) For one full year after irradiation, the net effect was an increase in Float-Zone cell performance. The measurements in the current reporting period ($\sim$ 490 days after irradiation) show a possible slight redegradation in these cells. The performance is still the same as in the previous readings, however, within the experimental uncertainty.

All four of the Group 3 cells showed significant redegradation between the fourth day after bombardment (March 10, 1967) and the 240th day (November 1967). In cell TI 127 this redegradation continued between the 240th and the 360th day to the extent that the value of P_{max} on the 260th day approximated that obtained one hour after bombardment. The value of P_{max} for the other Group 3 cells have remained constant within experimental error since the 240th day. It is noted that three of the four cells in Group 3 were Lopex cells and that the cell suffering the least severe degradation was cell TI 166, the Float-Zone cell. From the 360th day (November 1967) to the present measurement (490th day), the performance of these cells have remained essentially constant.

Cells He 248P and 249P, with a highly doped-phosphorous region near the junction have displayed particularly good behavior after irradiation. Though pre-irradiation power values (8.4 mW/cm^2 in each cell) were low, the resistance of the cells to irradiation was high, as seen from the values one hour after bombardment. Recovery continued steadily with time. As of the latest reading, approximately 16 months after bombardment, the cells had values of 6.7 and 7.3 mW/cm^2 for P_{max} i.e., $\sim$40 percent above the value for a 10 Ω-cm n/p cell after bombardment at 10^{16} e/cm^2.

3. Cells Irradiated to 10^{15} e/cm^2 in November 1967

Performance characteristics of four similar TI cells which were irradiated to $\sim 10^{15}$ e/cm^2 are plotted in Figure 4. These cells were all fabricated from 20 Ω-cm Float-Zone silicon; the initial lithium densities, ~ 1 μm from the junction, were

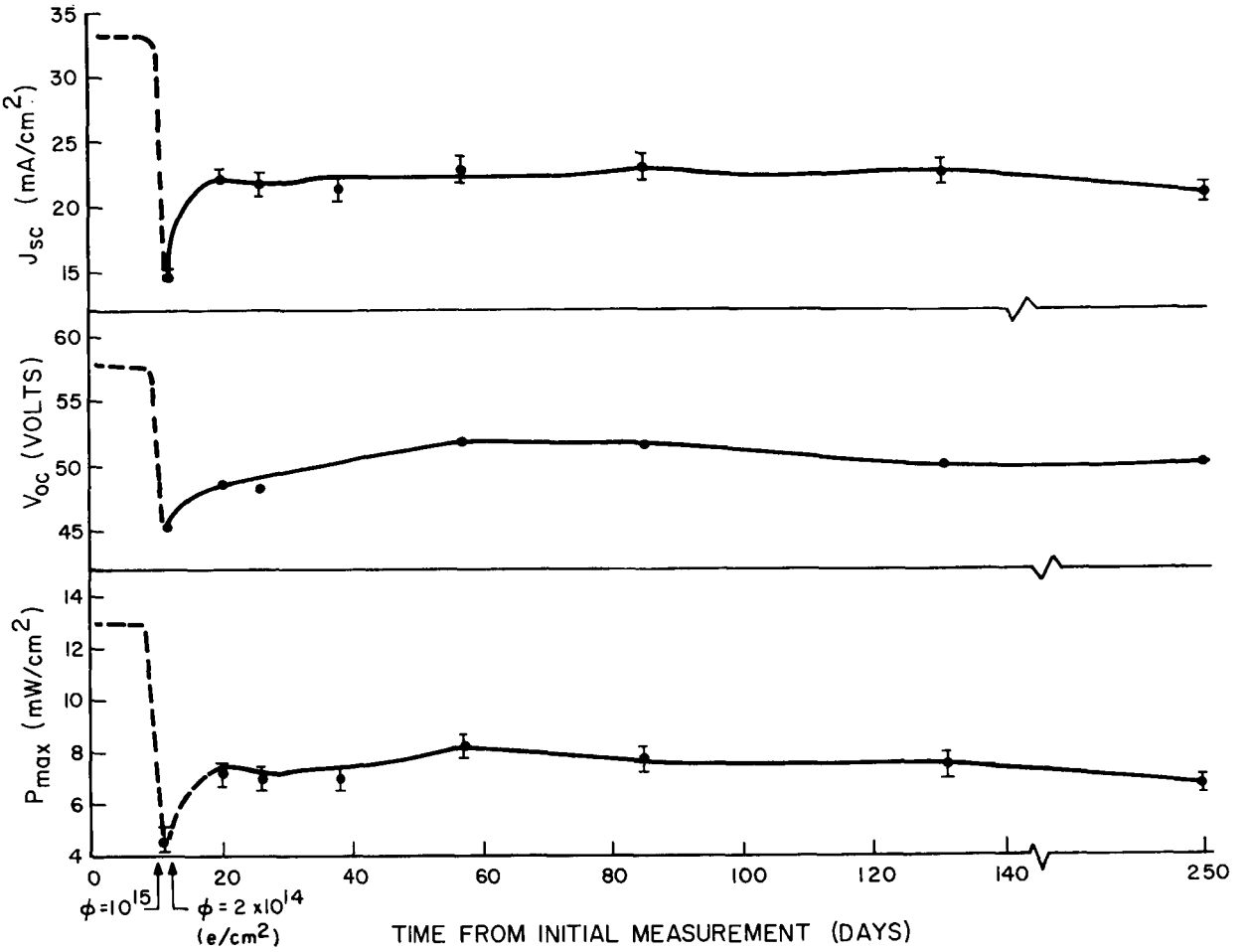

Figure 4. Stability Results from GFE Solar Cells Irradiated to 10^{15} e/cm^2

from 2 to 3 x 10^{15} cm. All have displayed similar behavior throughout their histories. In Figure 4, the values which are given are the averaged values of the four cells. All cells were made from 20 Ω-cm Float-Zone silicon and all displayed similar behavior. The "error bars" indicate the range of values obtained for the four cells rather than the experimental error of the measurement. Where no bar is shown, all values were essentially equal. The results show that the post-recovery values of all cell parameters remained substantially constant for a period of 120 days; no redegradation occurred. Between the 120th day of the tests and the July 1968 measurements (260th day), a slight, but less than 10 percent redegradation is seen to occur. In order to determine whether this redegradation is real or due to the experimental uncertainty in the measurement, future trends will be followed.

4. Cells Irradiated to 10^{14} e/cm^2 in November 1967/March 1968

This last group of cells, represented in Table IV, consists of four TI cells irradiated in November 1967 and nine He cells irradiated in March 1968. The full histories are given; the irradiation dates are indicated in the Table. Of the total of thirteen cells, eight were fabricated from 20 Ω-cm Float-Zone silicon, three from 200 Ω-cm Lopex silicon and two from 20 Ω-cm Lopex silicon. Comparing post-irradiation performance trends from a time one month after irradiation to a time four months after irradiation, it is seen that power redegradation in the five Lopex cells is significant, going from an average of 10.4 mW/cm^2 at one month to 8.3 mW/cm^2 at four months. This represents a 20-percent redegradation. (The one-month reading for He 670 was discounted as erroneous due to contact problems and not included in the average. This action was justified by the high value of J_{sc} obtained and the low filling factor obtained in this reading.) Likewise, the Float-Zone cells experienced redegradation from the first to the fourth month after irradiation, although to a lesser degree than the Lopex cells: 11.1 mW/cm^2 at one month to 10.1 mW/cm^2 at four months for an average of 10-percent redegradation.

Readings seven months after irradiation were obtained for the four TI cells. All of the cells show further redegradation since the four-month readings. The 20 Ω-cm Float-Zone cell, TI 952, showed a total redegradation of 25 percent from the first to the seventh month. The three 200 Ω-cm Lopex cells showed an average redegradation of 27 percent during the same period.

Pre-irradiation capacitance measurements showed that the lithium density at a distance ~1μm from the junction in these cells was in the range 1 to 3 x 10^{15} cm.

TABLE IV. CELLS IRRADIATED TO NOVEMBER 1967 AND MARCH 1968

Sample No.	P_o (Ω-cm) and Growth Method	October 1967		November 1967		December 1967		March 1968		March 1968		April 1968		July 1968	
		J_{sc}	P_{max}	J_{sc}	P_{max}	J_{sc}	P_{max}	J_{sc}	P_{max}	J_{sc}	P_{max}	J_{sc}	P_{max}	J_{sc}	P_{max}
TI 952	20 FZ	33.0	12.6*	[28.2]	[10.3]	30.0	11.1	28.9	10.2			30.4	10.4	27.7	8.5
977	200 L	34.3	12.0*	[28.4]	[9.5]	30.2	10.4	28.6	8.9			30.2	9.0	28.5	7.3
978	200 L	34.5	13.4*	[28.8]	[10.0]	30.6	10.3	29.2	8.5			30.7	8.5	27.0	6.5
981	200 L	35.5	12.4*	[29.5]	[10.0]	31.5	10.5	30.2	10.3			32.0	11.0	28.5	9.2
He 651	20 L			26.3	9.8			27.2	10.3 †	(23.9)	(8.9)	27.9	10.4	23.4	6.8
670	20 L			27.7	10.8			28.6	10.6 †	(24.7)	(9.5)	28.6	6.7	25.6	8.9
798	20 FZ			27.6	10.4			28.6	11.1 †	(23.4)	(8.5)	29.1	11.0	26.3	9.8
810	20 FZ			27.9	9.6			28.9	10.0 †	(24.1)	(8.1)	29.5	10.2	26.9	9.2
879	20 FZ			30.1	11.9			30.9	12.3 †	(25.0)	(9.2)	31.6	12.2	29.1	10.9
881	20 FZ			29.6	11.2			30.4	10.1 †	(25.5)	(8.4)	30.9	9.7	28.2	9.4
882	20 FZ			29.6	11.4			30.5	11.9 †	(25.1)	(9.0)	31.1	11.8	28.5	10.6
884	20 FZ			30.2	10.8			31.2	11.3 †	(25.1)	(8.6)	31.5	11.3	28.9	10.4
885	20 FZ			28.9	10.9			29.8	11.3 †	(24.6)	(8.8)	30.6	11.5	28.2	10.5

Notes: J_{sc} *is measured in mA cm*^{2}
P_{max} *is measured in mW cm*^{2}
* *Irradiated 8 November 1967*
† *Irradiated 12 March 1967*
[ ] *indicates post-recovery value, 8 days after bombardment*
( ) *indicates readings taken during recovery ~ 1 hour after bombardment*

D. STABILITY OF TEST DIODES

About thirty test-diodes fabricated by AED during the previous contract (Reference 4) have undergone diffusion-length stability tests over times ranging up to ~ 1 year. These tests had to be temporarily suspended due to instability problems with the Van de Graaff generator at the very low current densities ($\lesssim 10^{-9}$ A/cm^2) required for these measurements. It is expected that these problems will soon be solved and these tests will be reinstituted in the next reporting period. However, no striking redegradation of diffusion length has yet been observed in these devices.

E. DISCUSSION AND SUMMARY ON CELL STABILITY

In the discussion to follow, an attempt will be made, on the basis of the present limited statistics, to arrive at some tentative conclusions concerning stability of lithium cell performance relative to the physical parameters of the cells. Since the I-V characteristics carry a ±5 percent uncertainty, only excursions greater than 10 percent will be considered. Pre-irradiation stability and post-recovery stability after electron bombardment will be considered separately.

1. Pre-Irradiation Stability

Twenty-one cells, sixteen Float-Zone cells and five Lopex cells, have been monitored for a period of eight months. All of the cells made from Float-Zone refined silicon have maintained their initial power levels during this period. Three of the five Lopex silicon cells tested have degraded, these to the extent of 11, 10, and 30 percent. Evidently, the Float-Zone silicon cells have been superior to the Lopex cells in pre-irradiation stability.

2. Post-Recovery Stability

A total of 38 cells were tested, seventeen after 10^{14} e/cm^2, four after 10^{15} e/cm^2 and seventeen after 10^{16} e/cm^2. The general behavior in Float-Zone and Lopex cells is that an initial rapid recovery stage, encompassing 80 to 90 percent of the recovery, occurs in a time ranging from several hours to several days after irradiation ceases, that time depending upon the level of irradiation and the lithium density. This is followed by a steady but slower additional recovery, encompassing 10 to 20 percent of the recovery, and taking place over a time ranging from several weeks to several months, the time again depending upon the fluence and lithium density. After this time, either performance remains stable or redegradation begins. Measurements to date indicate that this critical stage is reached from approximately three to six months after irradiation.

By far the most severe redegradation was observed in cells irradiated to 10^{14} e/cm^2. Of the seventeen cells in this category, nine have redegraded, four of the five cells of Lopex silicon cells and five of the twelve cells of Float-Zone material. On the average, these lost $\sim$ 25 percent of their power output; one, a Float-Zone cell, lost $\sim$ 50 percent (probably due to contact problems). This amount of redegradation occurred $\sim$ 6 months after irradiation.

The four Float-Zone cells were irradiated to 10^{15} e/cm^2 appear to show signs of redegradation eight months after bombardment but, due to its slight extent ($\lesssim$ 10 percent) it is too soon to conclude for certain whether this is real or instrumental. No Lopex cells were irradiated to this level.

Of the seventeen cells irradiated to 10^{16} e/cm^2, the four cells with the highest lithium density showed redegradation. Three of these four are Lopex cells. Most of the remaining cells recovered to varying extents then stabilized. Exceptions to this are the three Heliotek cells with 100 Ω-cm starting material, which have redegraded over the last four months, due mainly to losses in the already low filling factor and the open-circuit voltage. The best stability and long-term recovery properties of the cells irradiated to 10^{16} e/cm^2 have been displayed by the two Quartz-Crucible cells (TI 112 and TI 113), which continue to recover after sixteen months and the two Float-Zone cells with a heavily-doped phosphorous layer at the p-n junction. Each cell (He 248P and He 249P) shows remarkable radiation resistance as well as stability (see 1-hour post-irradiation readings in Table III).

The tentative overall conclusions drawn from the above are:

(1) The stability of post-irradiation recovery after irradiation to a fluence of 10^{14} e/cm^2 presents a serious problem. This emphasizes the need for further extensive stability tests at low fluences.

(2) Greater stability, but, of course, less complete recovery is evidenced after higher fluences, 10^{15} to 10^{16} e/cm^2.

(3) Cells made from Float-Zone silicon appear to be more stable than cells made from Lopex silicon.

(4) The lithium density should be matched to the expected fluence. For example, three Hoffman cells with very low lithium density have shown excellent post-irradiation properties after 10^{14} e/cm^2. This would tend to indicate that the minimum amount of lithium compatible with a given fluence should be employed.

(5) The starting resistivity of the n-type material should not be too high if a high fluence is expected. This was exemplified in the poor recovery characteristics and low filling factor in three Heliotek cells made from 100 Ω-cm Float-Zone silicon which were exposed to 10^{16} e/cm^2.

(6) Quartz-Crucible cells and cells with a heavily doped phosphorus layer at the p-n junction show very good post-irradiation qualities and should be pursued further. Emphasis should be placed on improving pre-irradiation performance of such cells.

(7) Evidence beings to accumulate that at least a proportion of the "re-degradation" phenomenon is indeed linked to the presence of radiation-induced defects. That is, ordinary on-the-shelf degradation of unir-radiated cells is significantly less severe than redegradation after 10^{14} e/cm^2. Conversely, low levels of irradiation do not produce a stabilizing effect in the cells.

SECTION IV
MEASUREMENTS OF LITHIUM DIFFUSION CONSTANT

A. GENERAL

Work by the present authors and others leaves little doubt that the recovery of damage in lithium-doped silicon is controlled by the rate of diffusion of lithium ions. Thus, any direct measurement of diffusion properties of lithium in the devices in question may throw an important light on the recovery process and its optimization in silicon devices.

Mass transport of lithium at elevated temperatures has been observed previously in lithium drift-compensated devices and has been utilized to measure the mobility of lithium in these devices (Reference 16). These devices were very different from solar cells in that they consisted of a lightly doped p-type base into which a heavily doped, graded junction of lithium has been diffused. Lithium was the only n-type dopant present and the diffusion constant was obtained by measuring the rate of decrease in device capacitance as the lithium drifts into and compensates the boron doped base at temperatures in the 25 to 125 ^{o}C region. In such devices, the diffusion constant, D_F, of free lithium in silicon of high purity was found to be 2×10^{-14} cm^2/sec at room temperature (Reference 17). However, in less pure silicon, impurities (e.g., oxygen) were found to form chemical complexes with lithium, thereby reducing the effective lithium diffusion constant. This effect was variable from sample to sample. When studying the properties of individual lithium-doped devices, it is therefore advantageous to obtain direct measurements of the lithium diffusion constant for each sample used.

B. MEASUREMENT METHOD

In later stages of work on an earlier contract[3], the drift of lithium at room temperature in a junction field was observed and utilized for the first time to obtain a direct measurement of an effective lithium diffusion constant at the edge of the p/n junction depletion region in solar cells. A brief outline of the method is as follows: An initial measurement of cell capacitance at zero bias was obtained. Then a small d-c reverse bias was applied to the cell. (The bias level was 3 V in the experiments.) This bias was maintained steadily over a period of time (~10 minutes) except at periodic (~30 second) intervals when the bias was switched off and the capacitance at zero bias was measured. The bias was then immediately reapplied after the time

($\approx$ 1 second) required for the zero-bias reading. The change in zero-bias capacitance as a function of time under reverse bias together with a knowledge of the donor density profile in the region of the applied electric field enabled the calculation of the local lithium mobility, i.e., the mobility at the edge of the junction. The lithium diffusion constant could then be obtained by use of the Einstein relation.

C. THEORY

The electric field, $\mathcal{E}$, at the zero-bias junction edge is obtained from the donor density profile by

$$\mathcal{E} = \frac{e}{\epsilon} \int_{w_o}^{w_3} N_D dw \qquad (1)$$

where

e is electron charge

ϵ is permittivity of silicon

N_D is donor density

w_0 and w_3 are depletion widths at zero and 3-volts bias, respectively.

The rate of change of w_0 is obtained by differentiation of the equation for cell capacitance:

$$\left| \frac{dw_0}{dt} \right| = \frac{\epsilon A}{C_0^2} \frac{dC_0}{dt} \quad , \qquad (2)$$

where C_0 is the capacitance of the junction at zero bias and A is the cell area. A measure of the lithium mobility, μ_{L0}, at the junction edge is obtained through the relation

$$\mu_{L0} = \frac{1}{\mathcal{E}} \left| \frac{dw_0}{dt} \right| \quad . \qquad (3)$$

This method was applied to a total of twenty-five Lopex and Float-Zone test diodes of 10 and 30 ohm-cm starting material. In fourteen Lopex cells the values of diffusion constant ranged from 0.05 to 0.28 D_F; in eleven Float-Zone cells the values ranged from 0.10 to 1.0 D_F. Recovery experiments after a 1-MeV electron fluence of 10^{13} e/cm^2 were made on twelve of these diodes. Unexpectedly, the recovery rates obtained yielded a value for the diffusion constant of lithium in the bulk of the collection region of the cell which was close to D_F, the value for free lithium.

Since the values measured at the junction edge were generally well below this value, it was considered possible that the diffusion constant near the junction edge had been lowered due to a high density of crystal imperfections near the surface and the boron diffused region. Accordingly, during the present reporting period, the theory of the method has been generalized to consider the diffusion constant for larger distances into the base region. The measurement would be performed as follows: a reverse bias V_a is applied briefly and the measured capacitance, C_a, gives the depletion width, w_a, for this bias. A reverse bias, V_b, where $V_b > V_a$, is then applied steadily to the cell. Periodically, the bias is reduced, and the bias voltage for which the capacitance is equal to C_a is found. This bias voltage, the measuring bias, will increase from the initial value, V_a, as a function of time at bias V_b due to the drift of lithium across the plane at w_a. When the measuring bias is found, the cell is returned to the bias V_b. This procedure is repeated until a plot of measuring bias as a function of time is obtained.

The change in cell capacitance is given by

$$dC = \frac{dQ}{V} - \frac{Q}{V^2}\, dV \quad , \tag{4}$$

where

$$Q = e \int_{w_0}^{w_a} N_D\, dw$$

and

$$V = V_{p\text{-}n} + V_a \quad ,$$

and $V_{p\text{-}n}$ is the junction voltage at zero bias. Implicit in Equation (4) is the assumption that $C = Q/V$, which is strictly true only for a parallel-plate capacitor with no charge in the volume between plates. It does not apply to a p-n junction where $C = dQ/dV$

(Reference 18). However, for simple distributions, such as the linearly graded junction, this Equation is true to within a constant factor ($C = q/(3V)$ for a linearly graded junction). Most of the lithium cells tested previously exhibit a fairly good approximation to a linearly graded junction. Consequently, diffusion constant probes will be limited to cells which satisfy this condition. The correction factor will drop out of the Equation when $dC = 0$.

In the measurement, $dC = 0$, therefore, Equation (4) reduces to

$$dQ = \frac{Q}{V}\, dV \quad , \tag{5}$$

where dQ is the quantity of charge which has drifted across the plane at w_a with the cell at bias V_b. This quantity is also given by

$$dQ = e\mu\mathcal{E}N_{La}A\,dt \quad , \tag{6}$$

where N_{La} is the lithium density at w_a and $\mathcal{E}$ is found by integration of Equation (1) from w_a to w_b.

The lithium mobility is obtained from Equations (5) and (6) and the measured value of dV_a/dt.

D. STATUS

If a reduction in lithium diffusion constant indeed is found to occur near the junction, such an effect could be a very important factor in long-term stability of lithium doped devices since a local reduction in lithium diffusion constant at the junction would provide a "brake" for the unwanted flow of lithium across the junction, thereby increasing shelf and operating life. It is, therefore, important to obtain lithium diffusion-constant measurements in the bulk of the base region, away from the junction. This is difficult due to the high reverse biases required, but experiments are being made with circuits and bias schedules on lithium cells with suitable doping profiles.

SECTION V

LOW-TEMPERATURE MEASUREMENTS

A. BULK SAMPLES

1. General

During bombardment of silicon crystals by high-energy particles, the first defects formed are simple and intrinsic to the silicon lattice. These primary defects consist of vacancy-interstitial pairs. The free interstitial is mobile at temperatures as low as 4°K and the vacancy is mobile to temperatures of 77°K. Studies of primary defect formation during low-temperature electron bombardments of n-type silicon crystals have been reported in the literature (Reference 19). Such low-temperature studies are necessary to understand the mechanism of production of primary defects and their subsequent reactions. The reaction products, or secondary defects, are formed during thermal reordering processes. Electrical properties of solar cells irradiated by electrons of moderate energies (1 to 2 MeV) are dominated by the secondary defects formed by the interaction of primary defects with impurities in the crystal. For example, the silicon A-center is a defect-impurity complex consisting of an oxygen ion and a vacancy. In general, impurities are immobile at or below room temperature. However, lithium is an impurity which is highly mobile at room temperature and this mobility makes it possible for lithium to diffuse to and complex with radiation-induced defects. However, at a temperature of about -10°C, lithium is virtually "frozen" in the silicon lattice. Thus, by irradiating samples at temperatures at which the vacancy is immobile and then raising the temperature, it will be possible to investigate the steps by which lithium interacts with the primary and secondary defects.

In the paragraphs that follow, the results of Hall-effect and electrical-conductivity measurements on electron-irradiated silicon doped with lithium will be presented. Information on the damage mechanisms in silicon maintained at bombardment temperatures ranging from 79°K to 280°K will also be given. The Hall-effect and resistivity measurements were used to monitor carrier-removal rates as a function of bombardment temperature and were also used to monitor the isochronal annealing of defects over a temperature range from the lowest bombardment temperature of 79°K to 280°K.

2. Experimental Techniques

The Hall-effect and resistivity measurements were obtained by applying direct current-voltage techniques on Hall bars of lithium-doped n-type Quartz-Crucible silicon. As of the end of this reporting period, two samples, described in Section II, have been irradiated, however data reduction and analysis of the experimental results have not been fully completed.

A cross-section of the irradiation apparatus is shown in Figure 5. The principle parts of the apparatus are identified by letters in the illustration. Section A and B are reservoirs for the liquid nitrogen. The lower portion of the apparatus has two copper radiation shields. One extends downward from A and the other, D, surrounds the specimen. The sample mounting strip, F, shown in detail in Figure 6, contains two holes. The specimen is mounted in one and a copper strip with a calibrated hole size, equivalent to the rectangular area which the specimen occupies, is mounted in the other. Either one of these holes can be positioned in the electron beam by means of the double bellows G, and spring P. The spring is able to support the structure in its upper position when the space between the bellows is filled with air at atmospheric pressure. When this space is evacuated by a forepump, the bellows contracts and lifts the inner dewar, and, therefore, the sample holder to the second position. The system can be cycled rapidly between these two positions by means of an electrically operated valve which alternately exposes the space between the bellows to the atmosphere and to the forepump vacuum. The magnetically operated shutter, L, is used to interrupt the beam without shutting off the machine, deflecting the beam, or disturbing the setup in any way. When the beam is cut off, the sample is dropped into place by activating the 3-way electrically operated solenoid valve which exposes the bellows, M, to the air. An electromagnet, O, with an axis concentric with the beam, permits measurements of the Hall coefficient without disturbing the sample. The inside of the apparatus is evacuated by means of the vacuum pumping system of the electron accelerator through the opening where the apparatus is joined to the beam tube.

A 1-MeV Van de Graaff accelerator was used as the electron irradiation source. The electron flux was measured by positioning the Faraday cup, H, directly behind the space occupied by the hole in F. The cup is insulated by a lavite washer, R, and has a current lead attached to it via the glass seal, S. The uniformity of the beam at the specimen position was checked in the following manner: The beam current was first maximized electrically by adjusting the magnetic lens and the voltage deflection plates. At the "closed" end of the Faraday cup, a trap door, J, was suspended across an opening. A hollow tube, I, which contained a thin phosphor screen, T, across one end could be moved through J when a soft iron washer, attached at its opposite end, was moved forward by successively switching on a set of electromagnets wound around in coil form. The phosphor screen was then moved forward until it was directly behind the position reserved for the sample. When the electrons struck the phosphor it fluoresced. The resulting pattern was viewed by a television camera which was

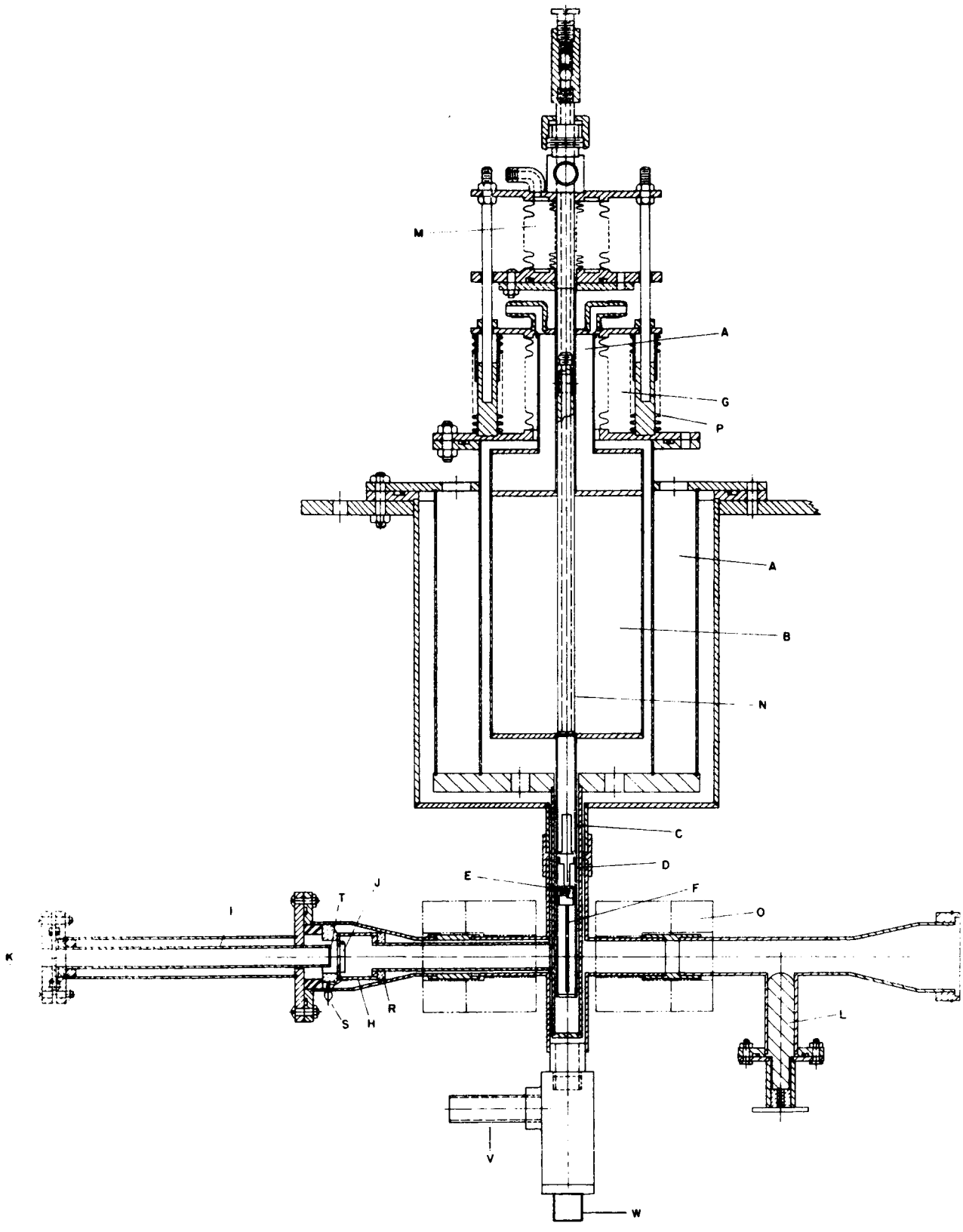

Figure 5. Cross-Section of Irradiation Apparatus

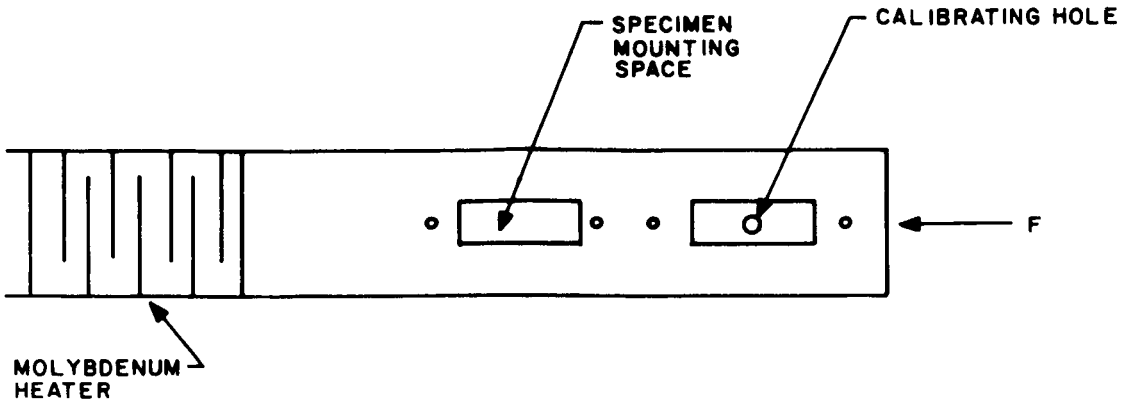

Figure 6. Sample Mounting Strip

positioned behind the window, K. Any necessary focusing or deflection was made and then the tube, I, was withdrawn from the Faraday cup. The trap door, J, was closed and the beam current passing through the hole in F could be measured. The sample leads were brought out of the apparatus through the side arm, V, below the sample as shown in Figure 5. A quartz glass window, W, located below the lead feed-through was used to illuminate the sample with white tungsten light to check for trapping effects.

3. Experimental Results

Electron irradiation of n-type silicon introduces defects which can accept electrons from the conduction band. Thus, carriers are removed and charged scattering centers are created which reduce the electron mobility. Both the loss of carriers and the reduction of mobility cause the resistivity of the silicon to increase. The effects were separated by measuring both the resistivity and the Hall coefficient.

Carrier-removal results obtained on Sample No. 1 are shown in Figures 7 and 8 for two bombardment temperatures of 79°K and 250°K. All measurements of carrier-removal rates were made at 79°K. As is customary, a carrier-removal rate was calculated from the slopes ($-\Delta n/\Delta\Phi$) of the straight-line fits to the data. Two separate irradiations were carried out at T_B = 79°K and one run at the high temperature of T_B = 250°K. After the completion of each irradiation run, annealing-rate and temperature-dependence measurements were made. The high-temperature limit was chosen to be 250°K so that the mobility of the lithium ions was at no time greater than 1/50 of the room temperature value. By setting this temperature limit, the interaction of lithium with radiation-induced defects was reduced to a negligible amount. The carrier-removal rates at low and high temperatures were determined to be 0.036 and 0.4 cm^{-1}, respectively. The exponential dependence of carrier-removal rate on bombardment temperature in phosphorus-doped silicon has been reported in the literature (Reference 19) and the order of magnitude difference in the removal rates was expected.

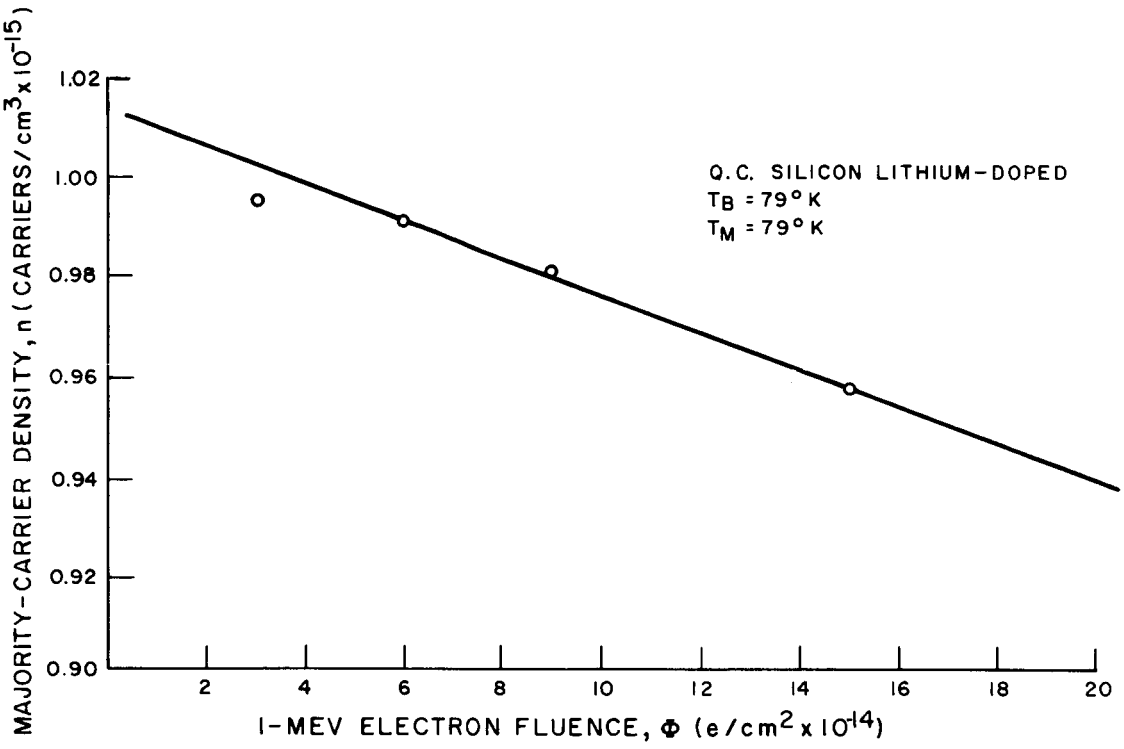

Figure 7. Carrier Removal at 79°K vs. Bombardment Fluence at 79°K

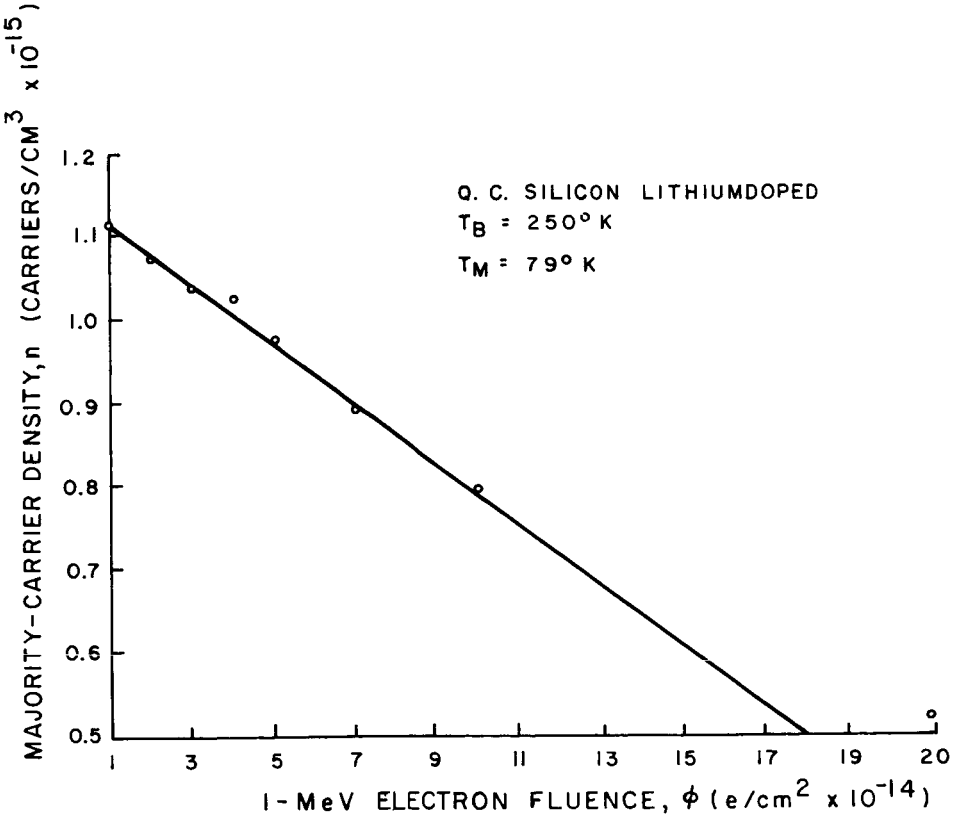

Figure 8. Carrier Removal at 79°K vs. Bombardment Fluence at 250°K

After the completion of the low-temperature bombardments (T_B = 79°K), an isochronal annealing run of ten minute duration at each annealing temperature was carried out. The product of the unannealed fraction and $\Delta n/\Delta\Phi$ is shown in Figure 9 for one of these experiments. Similar results were obtained in all annealing measurements. There appears to be two annealing stages (I and II) and a reverse annealing peak at 250°K which has been observed in other electrical experiments. (Reference 19) Following the description of Vook and Stein (Reference 19), of silicon without any lithium content, the first stage is considered to be independent of lithium and due to the annealing of ITI (Irradiation-Temperature Independent) defects in the temperature range of 100°K to 200°K. The second stage is not as distinct but appears to occur at $\approx$ T = 180°K. At this time, there is no identification of this defect. Vook and Stein attributed the reverse-annealing peak to the formation of a defect located at an energy of 0.13 eV below the conduction band. This reverse annealing peak is not observed in oxygen-lean Float-Zone silicon, and thus, the production of this defect requires the presence of oxygen. The carrier-removal rate increased by $\sim$ 100 percent in the temperature range of 220°K to 250°K. The separation of the total carrier-removal rate into its separate component rates can be deduced from the annealing cycle. Thus 0.02 cm^{-1} is attributed to ITI defects, and 0.016 cm^{-1} to ITD (Irradiation-Temperature Dependent). The ITD defects are those which involve impurities such as oxygen, phosphorus, or lithium. In the present case, the phosphorus background is quite low, ($\approx 10^{14}$ P/cm^3), thus E-centers are not likely to occur. The two possibilities are the A-center (O-V) or a center involving lithium. More will be said about this latter possibility after all the experimental results have been analyzed. Correlation of carrier-density changes with changes in mobility μ during the annealing cycle is indicated in Figure 9 where the unannealed fraction of reciprocal mobility, is plotted as a fraction of annealing temperature. The annealing cycle of $1/\mu$ values shows only a single stage of annealing, but the reverse-annealing peak at T = 250°K is in agreement with the behavior of the carrier-removal rate, $\Delta n/\Delta\Phi$.

Sample No. 2 was bombarded at seven different temperatures and the loss in carrier density versus fluence was measured. All electrical measurements were made at a standard temperature of 79°K. After each set of irradiations and measurements were made at any bombardment temperature, the sample temperature was increased to 200°K and maintained at this temperature for 30 minutes. Following this annealing period, the sample temperature was decreased to 79°K and measurements of carrier density were again made. The unannealed fraction of carrier density was calculated and used to determine the irradiation-temperature-dependent (ITD) carrier-removal rate, $\Delta n/\Delta\Phi$. This corrected carrier-removal rate for the production of ITD defects versus bombardment temperature is shown in Figure 10. The solid curve is drawn through the experimental points, and the dashed curve though calculated points using the probability of defect formation P_c indicated on the illustration. This is the expression used in Reference 19 to fit the experimental data and described in a later section. However, this data is best fitted by a metastable-pair energy level located at E_c-E_M = 0.06 eV instead of 0.07 eV used in Reference 19. The reverse annealing peak observed in Figure 9, at T_a = 250°K, is due to the introduction of an additional carrier removal defect and is also observed in Figure 10 at a bombardment temperature of T_B = 250°K.

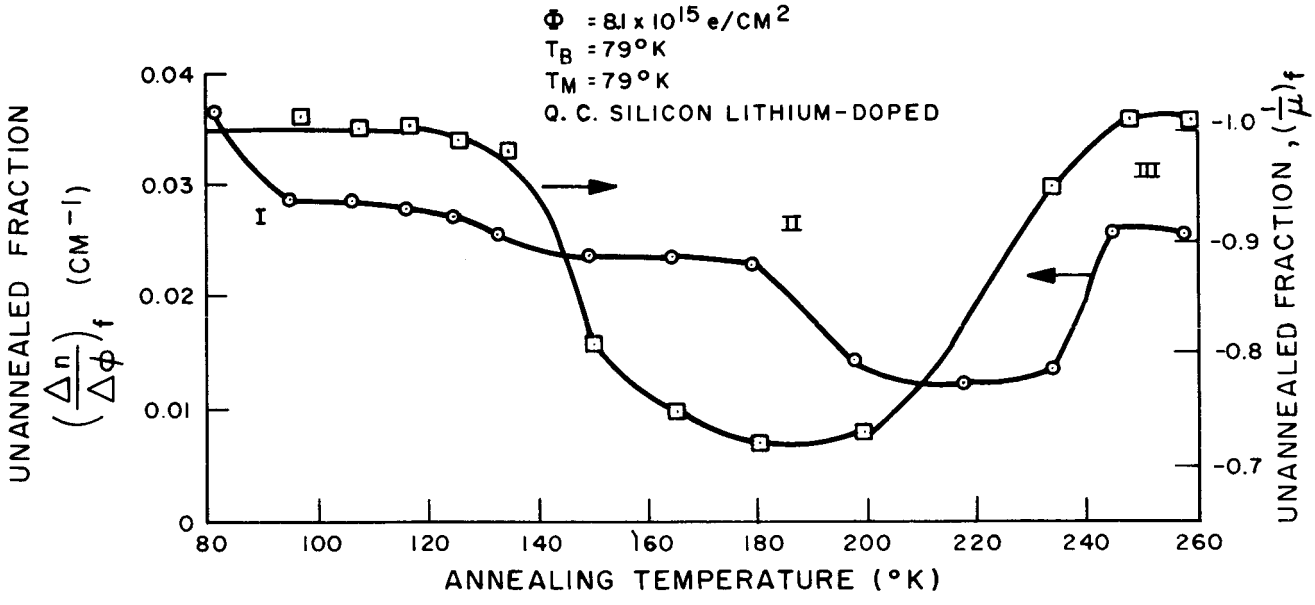

Figure 9. Unannealed Fraction of Carriers Removed and Unannealed Fraction of Reciprocal Mobility as Functions of Annealing Temperature: All Measured at 79°K

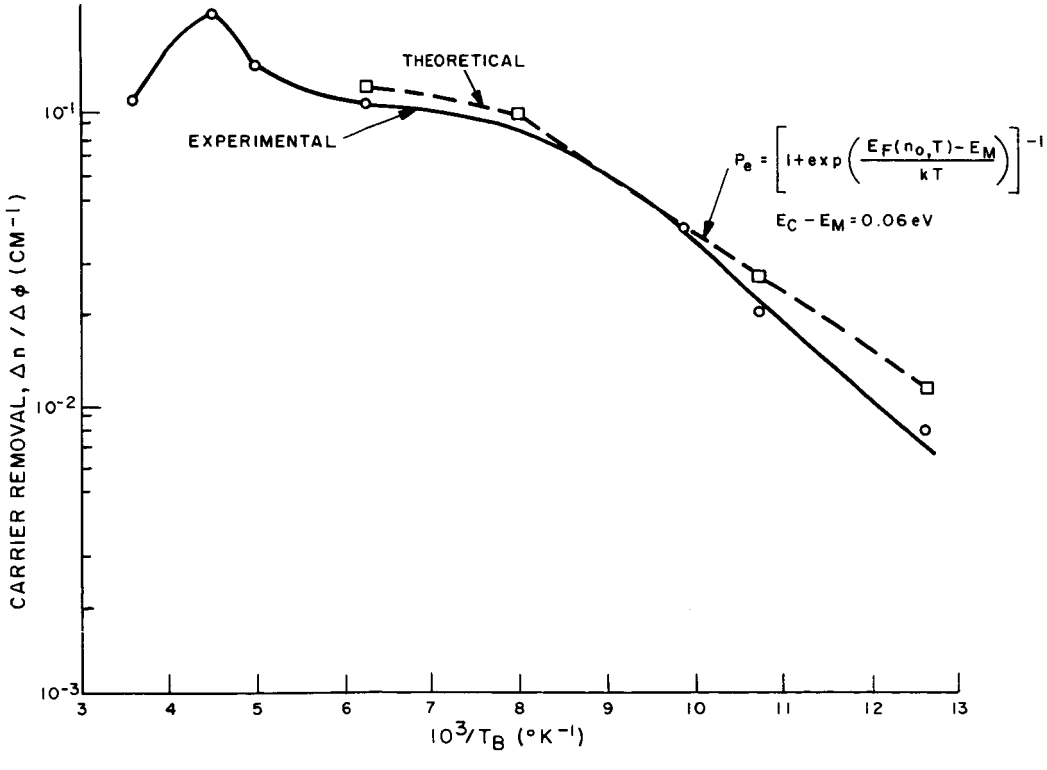

Figure 10. Corrected Carrier Removal Rate vs. Bombardment Temperature

4. Discussion of Results

a. Stein's Model

As the results obtained on Quartz-Crucible silicon in this and other experiments are consistent with a model generated by Stein (Reference 19), a brief statement of the theory is included. The theory predicts a temperature-dependent probability for the formation of complexes between oxygen and separated close-spaced vacancies and interstitials. Based on this model, in its simplest form, the probability of defect formation is given by

$$P_c = \left[1 + g \exp \left\{ \frac{E_F(n_0, T_B) - E_M}{k T_B} \right\} \right]^{-1} \qquad (7)$$

where

g is the ratio of the number of ways the state can be occupied to the number of ways the state can be unoccupied.

$E_F(n_0, T_B)$ is the Fermi energy level for electrons and is a function of the initial carrier concentration, n_0, and bombardment temperature, T_B.

E_M is the energy level of the metastable interstitial vacancy pair.

The location of the Fermi level can be determined from the pre-irradiation carrier density versus temperature curves. E_M is an empirical constant obtained from the limiting slope of carrier-removal rate versus bombardment temperature curves.

The annealed fraction of carrier-removal rate $\Delta n/\Delta \phi$ and reciprocal of mobility were used in presenting the data in Figure 9. Equations (8) and (9) were used to compute the annealing curves shown in Figure 9.

The unannealed fraction of $\Delta n/\Delta \phi$ is given by

$$\left(\frac{\Delta n}{\Delta \phi}\right)_f = \frac{n_{T_A} - n_0}{n_{T_B} - n_0} \left(\frac{\Delta n}{\Delta \phi}\right)_{T_B} \quad (CM^{-1}) \qquad (8)$$

where

n_{T_A} is the carrier density observed after annealing at the temperature T_A

n_0 is the pre-irradiation carrier density

n_{T_B} is the carrier density after bombardment at temperature T_B

$\left(\frac{\Delta n}{\Delta \phi}\right)_{T_B}$ is the carrier removal rate measured at bombardment temperature T_B.

The unannealed fraction if $1/\mu$ is given by

$$\frac{1}{\mu_f} = \frac{\frac{1}{\mu_{T_A}} - \frac{1}{\mu_0}}{\frac{1}{\mu_{T_B}} - \frac{1}{\mu_0}} \tag{9}$$

where the values of Hall mobility, μ, in Equation (9) are defined in the same manner as those for n in Equation (8).

b. Analysis of Results

Results for only two bombardment temperatures at $T_B = 79°K$, and 250°K were obtained on Sample No. 1. These results indicated that the production rate of carrier-removal defects was considerably reduced at low bombardment temperatures. The experimental ratio of carrier-removal rates at $T_B = 250°K$ and 79°K is 13 (0.2/0.16), where the contribution of the defect due to the reverse annealing peak was subtracted from the total $\Delta n/\Delta\phi$ of 0.4 cm^{-1}. Calculation of this ratio based on the semi-emprical Equation (7), and a metastable-pair energy level located at an energy of $E_c - E_M = 0.06$ eV is 15. Thus, the present temperature-dependence results are in close agreement with those of Reference 19, obtained on phosphorus-doped Quartz-Crucible silicon of 10 Ω-cm resistivity. Sample No. 2 was approximately a factor of ten greater in lithium doping density ($\rho = 0.3$ Ω-cm) than Sample No. 1. It was expected that the limiting slope of the $\Delta n/\Delta\Phi$ versus temperature curve would shift along the temperature axis toward lower temperatures. Thus, the sample with lower resistivity would have a lower value of $\Delta n/\Delta\Phi$ at the lower temperature than the sample with higher resistivity. It was observed that $\Delta n/\Delta\Phi = 0.008$ cm^{-1} for Sample No. 2 as compared with 0.016 cm^{-1} for Sample No. 1 at a bombardment temperature of $T_B = 79°K$, which is in agreement with the theoretical predictions.

The best fit of the data obtained on Sample No. 2 and shown in Figure 10, was accomplished by locating the energy level of the metastable-pair defect at 0.06 eV below the conduction band. This disagrees with the value of 0.07 eV found in the literature for 1-10 Ω-cm quartz-crucible silicon doped with phosphorus. However, Vook and

Stein found a variation among different samples of 0.05 to 0.07 eV and our value falls within this range. The additional defect which is produced when the sample temperature is raised to 250°K is not accounted for in the model described by Equation (7) for the probability of defect formation, P_c. Thus, Equation (7) does not predict the peak of $\Delta n/\Delta\Phi$, which occurs at 250°K, but predicts a saturation of the carrier-removal rate as the bombardment temperature is increased. The absolute value of the carrier-removal rate at T_B = 250°K was approximately a factor of two greater for Sample No. 1 than for Sample No. 2. The values of both samples are smaller than those of Reference 19. The significance of the difference cannot be explained at this time. Future measurements may provide the explanation.

5. Conclusions

The formation of carrier-removal defects in lithium-doped Quartz-Crucible silicon bombarded by electrons is inhibited at low bombardment temperatures. A model of secondary-defect production from primary metastable-pairs (interstitial and vacancy) appears to adequately fit the dependence of carrier-removal rate on bombardment temperature previously proposed in Reference 19. Two types of defects are produced at bombardment temperatures less than 200°K: the ITI defect (Irradiation-Temperature Independent) and the ITD defect (Irradiation-Temperature-Dependent). The results obtained on Sample No. 2 showed that the carrier-removal rate due to ITI defects was independent of bombardment temperature and equal to a value of 0.003 cm^{-1}. This value disagreed with the value of 0.02 cm^{-1} obtained on Sample No. 1. There is no explanation at the present time to explain this discrepancy. Future measurements on additional samples of moderate and high lithium-doping densities and further reduction of all data obtained on Samples 1 and 2 may provide an explanation.

B. SOLAR CELLS

1. General

These experiments provide a logical follow-on and extension of the room-temperature recovery experiments performed last year (Reference 4). Their purpose is, in conjunction with the low-temperature bulk-sample measurements, to obtain interrelated information concerning the physical mechanisms operative in the cell. The motion of vacancies and of lithium can be essentially frozen at liquid-nitrogen temperatures. If the radiation damage is introduced at this temperature, the subsequent interactions of phosphorus, lithium, oxygen, and vacancies, the reactions of which are very rapid at room temperature, can be slowed to the desired rate by careful temperature control. They can then be monitored carefully and sequentially. The temperature dependence of each stage also provides basic data on the defect energy levels and diffusion barriers involved.

2. Construction of Vacuum-Cold Finger

A cold-finger apparatus, for measurement of cell parameters at temperatures ranging down to that of liquid nitrogen, has been designed to fit onto the electron-beam exit flange of the Van de Graaff Generator. Briefly, the apparatus, shown schematically in Figure 11, consists of a cold finger, F, enclosed in a vacuum-tight chamber, C. The finger consists of a rectangular 1- by 2-inch waveguide, W, 13-3/4 inches long, 12 inches have been milled off of each of three sides, leaving a 1-3/4-by 1-inch extension which serves as the cold finger. Cells or test-diodes, D, are mounted at the end of this finger via the metallized boron-nitride wafer described in Section III. Metallized Alundum heaters are mounted on the back of the finger. The waveguide is closed by a brass plug, P, at either end; at the top, a stainless-steel tube, T, runs from the plug to a flange, F_1. Liquid nitrogen is poured into the waveguide through T_1. The flange has electrical feed-throughs for heater, cell, and thermocouple leads and a mechanical feed-through that enables vertical movement of a 0.012-inch aluminum moderator, M_1, used in electron-voltaic diffusion-length measurements. The cold finger fits into a larger, 3- by 1-1/2-inch waveguide; a vacuum (0-ring) seal is made between W_1 and W_2, the latter being the flange on the larger waveguide. The large waveguide contains a Faraday cup, FC, for electron flux measurements, and a mechanical feedthru, M_2, which enables horizontal movement of a 0.095-inch aluminum plate which shields the cell from the beam when desired. A tube, T_2, connects with the vacuum pump. The entire assembly is attached to the beam exit flange through a mating flange, F_2, on the large waveguide. A hole in the shape of a "T" was milled in the large waveguide near the center of F_2 to permit access of the electron beam to the sample and Faraday-cup areas. Vacuum seals to the beam exit flange are made by two neoprene gaskets and a 0.001-inch aluminum window.

The cell parameters to be measured in this apparatus are capacitance vs. reverse bias, diffusion length, and possibly minority carrier lifetime. Attempts will be made to correlate these measurements with the Hall measurements now being made.

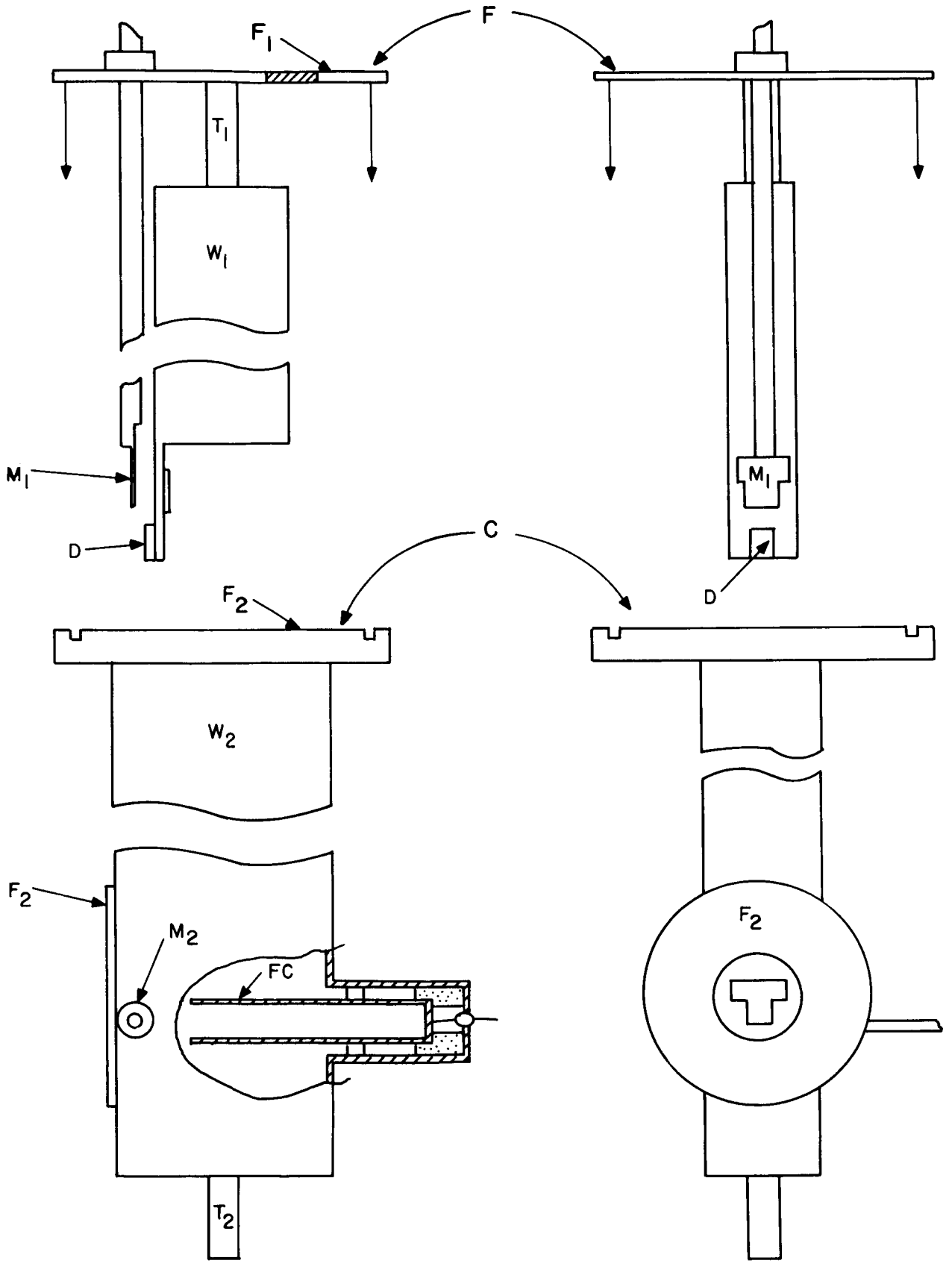

Figure 11. Cold-Finger Apparatus, Schematic Diagram

SECTION VI

CONCLUSIONS AND FUTURE PLANS

A. CONCLUSIONS

1. Stability

Stability data are now available for some cells for periods ranging to approximately two years. The post-irradiation data, obtained after fluences of 10^{14}, 10^{15}, and 10^{16} e/cm^2, indicates that post-recovery redegradation is most severe after 10^{14} e/cm^2. After 10^{15} and 10^{16} e/cm^2, recovery is less complete but redegradation less severe. Over an 18-month period, redegradation phenomena in lithium-containing solar cells can vary from insignificant in magnitude to very serious. The time period from approximately three to six months after recovery seems to be critical with respect to redegradation. The type of silicon and its processing are both very important. A definite superiority of Float-Zone-refined silicon over Lopex silicon is seen; the few samples tested indicate that Quartz-Crucible silicon, while producing a much slower recovery than the other two types, shows minimal redegradation over 18 months. High lithium concentrations are definitely to be avoided. The tests, in fact, indicate that the minimum amount of lithium consistent with the expected fluence should be used. However, much further work is needed to ascertain the nature of the redegradation phenomenon, e.g., precipitation or migration, due to its sporadic and variable occurrence.

2. Lithium Diffusion Process

It is not yet clear how the measured diffusion constant of lithium near the junction is related to that deduced for the whole (~200-micrometer) collection region of the cell. It appears that lattice damage is present in the junction depletion region even before irradiation and that this can be useful in stabilizing lithium in the cell. A method for extending lithium diffusion-constant measurements further into the base region has been developed. Planned low-temperature, high-bias measurements on devices should elucidate these questions as well as several questions on the kinetics of recovery of damage in lithium-containing solar cells.

3. Interaction of Lithium with Defects

Hall and resistivity measurements indicate that carrier-removal rates at low temperatures are lower in lithium-doped silicon than in phosphorus-doped silicon,

which also contains oxygen. This may mean that the affinity of vacancies for lithium is less than that for phosphorus, a fact which is in agreement with earlier experiments on recovery of solar cells (Reference 4). The more probable reason is the difference in the location of the Fermi level in the phosphorus-doped samples as compared to its location in the lithium-doped sample. A more complete explanation should be possible when the recently acquired data have been reduced and correlative measurements on solar-cells and test-diodes have been made. The interaction of lithium with vacancies has definitely been observed in recent work and the data will be of great use in improving and detailing the current models for damage to solar-cell performance at any temperature.

B. FUTURE PLANS

1. Hall Measurements on Diodes and Bulk Samples Containing Lithium

Low-temperature measurements on special lithium diodes made from the same ingots as Hall bars used in this quarter will enable majority-carrier removal and minority-carrier recombination phenomena to be correlated at all relevant temperatures.

2. Stability Tests on Test-Diodes and GFE Solar-Cells

Continuing evaluations will be made on solar-cells and test-diodes irradiated under the previous (NAS 10239) contract. Tests will also continue on unirradiated cells and diodes. Whenever feasible electron-voltaic diffusion-length measurements will be made in addition to measurements of photovoltaic I-V characteristics.

Irradiations and stability tests will be initiated on a new set of GFE cells.

3. Capacitance Measurements

Extensions of the capacitance measurements to cover a greater reverse-bias range will be attempted with cells at low temperatures. Diffusion-constant measurements extending into the bulk of the base region will be initiated.

LIST OF REFERENCES

1. J. J. Wysocki, P. Rappaport, E. Davison, R. Hand, and J. J. Loferski, Appl. Phys. Letters 9, 44 (1966).

2. T. R. Waite, Phys. Rev. 107, 463 (1957).

3. T. J. Faith, G. J. Brucker, A. G. Holmes-Siedle, IEEE Nuclear and Space Radiations Effects Conf. Missoula, Mont., July 1968, to be published in IEEE Trans. on Nuclear Sci.

4. G. Brucker, T. Faith, and A. G. Holmes-Siedle, Final Report on Contaact No. NAS-10239, prepared by RCA and issued March 8, 1968.

5. L. Valdes, Proc. IRE 42, 420 (1954).

6. W. Rosenzweig, Bell Sys. Tech. Journ. 41, 1573 (1962).

7. P. Payne, G. Goddelle, E. L. Ralph, NASA Contr. No. NAS5-10272.

8. D. Kendall and R. Vineyard, NASA Contract No. NAS5-10274.

9. P. Iles, NASA Contract No. NAS5-10271.

10. J. Hilibrand and R. D. Gold, RCA Rev. XXI, 245 (1960).

11. J. J. Wysocki, G. J. Brucker, A. G. Holmes-Siedle, RCA Annual Progress Rept., Contr. NAS5-10239 (June 1967).

12. R. L. Statler, NRL Rept. 6091 USNRL, Washington, D.C. (October 1964).

13. J. Mandelkorn, Sixth Photovoltaic Specialists Conf., Cocoa Beach, Fla., (March 1967).

14. E. M. Pell, Solid-State Electronics and Communications, p. 261, Eds. Desirant and Michels, Academic Press, New York (1960).

15. J. R. Carter, Jr., IEEE Nuclear and Space Radiation Conf., Columbus, Ohio, (July 1967).

16. E. M. Pell, J. Appl. Phys. 31, 291 (1960).

17. E. M. Pell, Phys. Rev. 119, 1222 (1960).

18. A. K. Jonscher, Principles of Semiconductor Device Operation, Wiley, New York (1960).

19. H. J. Stein and F. L. Vook, Phys. Rev. 163, 790 (1967).